Characterization of the Voltage-dependent Properties of a Volume-sensitive Anion Conductance

PAUL S. JACKSON* and KEVIN STRANGE‡

From the Critical Care Research Laboratories, Departments of *Neurosurgery and ‡Medicine (Nephrology), Children's Hospital and Harvard Medical School, Boston, Massachusetts 02115

ABSTRACT Outwardly rectified, swelling-activated anion conductances have been described in numerous cell types. The major functional variable observed amongst these conductances is the extent and rate of depolarization-induced inactivation. In general, the conductances can be divided into two broad classes, those that show rapid inactivation in response to strong depolarization and those that show little or no voltage dependence. The swelling-activated anion conductance in rat C6 glioma cells is inactivated nearly completely by membrane depolarization above +90 mV and reactivated by membrane hyperpolarization. The kinetics of inactivation and reactivation are fit by single and double exponentials, respectively. Voltage-dependent behavior is well described by a simple linear kinetic model in which the channel exists in an open or one of three inactivated states. pH-induced changes in voltage-dependent gating suggest that the voltage sensor contains critical basic amino acid residues. Extracellular ATP blocks the channel in a voltage-dependent manner. The block is sensitive to the direction of net Cl^- movement and increases open channel noise indicating that ATP interacts with the channel pore. Blockage of the channel with ATP dramatically slows depolarization-induced inactivation.

INTRODUCTION

Animal cells respond to swelling by activating volume regulatory mechanisms that mediate the net efflux of intracellular electrolytes (Hallows and Knauf, 1994) and small organic solutes termed organic osmolytes (Garcia-Perez and Burg, 1991; Yancey, 1994). Swelling-induced organic osmolyte efflux is mediated by an outwardly rectified, volume-sensitive anion channel termed VSOAC (Volume-Sensitive Organic osmolyte/Anion Channel; Strange, 1994; Jackson, Morrison, and Strange, 1994; Strange and Jackson, 1995). Swelling-activated whole-cell anion conductances with characteristics nearly identical to those of VSOAC have been observed in numerous mammalian cell types (reviewed by Strange and Jackson, 1995), in *Xenopus* oocytes (Ackerman, Wickman, and Clapham, 1994), and recently, in hepatocytes of the skate *Raja erinacea* (Strange, Churchwell, Ballatori, Boyer, and Jackson, 1995). The major

Address correspondence to Dr. Kevin Strange, Children's Hospital, Division of Nephrology, Enders 12, 300 Longwood Avenue, Boston, MA 02115.

J. GEN. PHYSIOL. © The Rockefeller University Press · 0022-1295/95/05/0661/17 $2.00
Volume 105 May 1995 661–677

functional variable observed amongst these conductances is the extent and rate of depolarization-induced inactivation. For example, anion currents in airway and intestinal epithelial cells (McCann, Li, and Welsh, 1989; Worrell, Butt, Cliff, and Frizzell, 1989; Solc and Wine, 1991; Chan, Goldstein, and Nelson, 1992; Kubo and Okada, 1992) and human keratinocytes (Rugolo, Mastrocola, De Luca, Romeo, and Galietta, 1992) show rapid inactivation at membrane potentials $> +60$ mV. In contrast, swelling-activated anion currents in human neutrophils (Stoddard, Steinbach, and Simchowitz, 1993), human and mouse T cells (Lewis, Ross, and Cahalan, 1993), canine cardiac cells (Tseng, 1992), a neuroblastoma × dorsal root ganglion cell hybrid (Pollard, 1993) and skate hepatocytes (Strange et al., 1995) exhibit very slow or no depolarization-induced inactivation.

Strong depolarization causes nearly complete inactivation of swelling-activated anion currents in rat C6 glioma cells. The purpose of the present study was to characterize this voltage-dependent behavior in detail. Our results provide a starting point for understanding cell-to-cell variability in the voltage-sensitivity of VSOAC.

MATERIALS AND METHODS

Cell Culture

Rat C6 glioma cells were cultured in Eagle's minimal essential medium (MEM; GIBCO-BRL, Gaithersburg, MD) with 10% fetal bovine serum (FBS) and penicillin/streptomycin as described previously (Jackson and Strange, 1993). The osmolality of the growth medium was elevated 24–48 h before the cells were used by adding NaCl directly to the MEM. The osmolalities of the normal and hypertonic growth media were measured using a freezing point osmometer (model Osmette A, Precision Instruments, Sudbury, MA) and were 295–300 mosmol/kg H_2O (mOsm) and 385–390 mOsm, respectively.

Patch Clamp Recordings

C6 glioma cells were grown on 12-mm diam glass cover slips, acclimated to 390 mOsm MEM for 24–48 h, and patch clamped in the whole-cell configuration at room temperature with symmetrical CsCl solutions as described previously (Jackson and Strange, 1993). Patch electrodes were pulled from 1.5 mm o.d. borosilicate glass microhematocrit tubes (Fisher Scientific, St. Louis, MO) that had been silanized with dimethyl-dichloro silane (Sigma Chemical Co., St. Louis, MO). The electrodes were not fire polished before use and had DC resistances of 3–5 MΩ. Cells were used only if the series resistance was < 10 MΩ.

An Axopatch 200A (Axon Instruments, Inc., Foster City, CA) patch clamp amplifier was used to voltage clamp C6 cells after gigaseal formation and attainment of whole-cell access. Command voltage generation, data digitization and data analysis were carried out on an 80486, 100 mHz IBM-compatible computer (Dell Optiplex 4100/MX, Austin, TX) using a DigiData 1200 AD/DA interface with pClamp software (Axon Instruments, Inc.). Electrical connections to the amplifier were made using Ag/AgCl pellets and 3 M KCl/agar bridges. Series resistance compensation of 70% was used for whole-cell recordings.

Computer Simulations

Simulation of voltage-dependent behavior was carried out using custom software written in BASIC. The response of 1,000 or 10,000 simulated channels to the voltage pulse protocols used in whole cell experiments (see Figs. 1 and 3) was calculated. All of the channels were set initially

in the open state at −80 mV. The state of each channel was then evaluated every 1 ms for 4 s. The probability that a channel would change state was determined using rate constants defined by Eq. 1 (discussed below). Resulting simulated current responses were then fit with single and double exponentials in the same manner as the whole cell current data. Kinetic parameters used in Eq. 1 were adjusted manually to obtain the best possible fit of the simulated currents to the observed whole-cell data.

Solutions

Cells were patch clamped with a pipette solution containing 140 mM CsCl, 2 mM $MgSO_4$, 20 mM HEPES, 6 mM CsOH, 1 mM EGTA, 0.5 mM GTP, 2 mM ATP and 50 mM raffinose (pH = 7.2; osmolality = 365–375 mOsm). The control bath solution contained 140 mM CsCl, 5 mM $MgSO_4$, 12 mM HEPES, 8 mM TRIS and 80 mM raffinose (pH = 7.4; osmolality = 385–390 mOsm). Cell swelling was induced by removing raffinose to reduce bath osmolality to 300 mOsm. Studies of extracellular ATP block were carried out by adding 10 mM Na_2ATP directly to the 300 mOsm bath solution and adjusting pH to 7.4 with CsOH. The effects of changes in extracellular pH on inactivation kinetics was studied using a HEPES/Tris or phosphate-buffered 300 mOsm bath solution.

RESULTS

Voltage-dependent Inactivation

Voltage-dependent gating kinetics were characterized in whole-cell currents since it is difficult to study individual VSOAC channels. As described in the previous paper (Jackson and Strange, 1995), membrane patches pulled from swollen cells generally contain more than a single channel. Furthermore, channels survive poorly in isolated patches (see Solc and Wine, 1991; Okada, Petersen, Kubo, Morishima, and Tominaga, 1994; Jackson and Strange, 1995), which makes it unfeasible to observe a large number of transitions necessary for statistical analysis of gating kinetics.

Cells were swollen by reducing bath osmolality 60–120 s after obtaining whole-cell access. As described previously (Jackson and Strange, 1993), VSOAC activates rapidly in response to cell swelling. After a stable current level was reached, the membrane potential was held at −50 or −80 mV and then stepped to test potentials of +50 to +120 mV in 10-mV increments. Each voltage step lasted 4 s and the cell was allowed to recover for 10–15 s at the negative holding potential before applying a subsequent voltage step. As shown in Fig. 1 *A*, current inactivation was observed at all potentials > +50 mV. The time course of current inactivation was well fit with a single exponential at all voltages tested (Fig. 1 *B*).

The mean time constant (τ) for inactivation is shown as a function of membrane voltage in Fig. 2 *A*. The τ increased from +50 to +70 mV and then progressively decreased with stronger depolarization. At +70 mV, the mean ± SE τ was 2,250 ± 280 ms (n = 6). The τ declined to 264 ± 25 ms (n = 6) at +120 mV.

Fig. 2 *B* shows the steady state level of current inactivation plotted as a function of membrane potential. The midpoint of the inactivation curve at which 50% of the current was inactivated was 70.1 mV. The extent of inactivation plateaued at voltages > +90 mV. At +120 mV, the whole-cell anion current was inactivated by 87 ± 2% (mean ± SE; n = 6). The nature of the remaining current is unknown at present. It

could be due to nonspecific leak, other active anion channels or a depolarization-induced subconductance state of VSOAC. In addition, the residual current may be due to a subpopulation of VSOAC that is not inactivated by depolarization. Whatever the nature of the residual current, it is clear that the majority of the swelling-induced anion current in C6 cells is due to the activity of VSOAC.

Voltage sensitivity is conferred by charged residues that move through the membrane potential field in response to changes in membrane potential. The steepness of the rising part of the curve describing the voltage dependence of inactivation (Fig. 2 *B*) is an indication of the amount of charge that moves through the membrane field during an inactivation event. The effective gating charge (Hille,

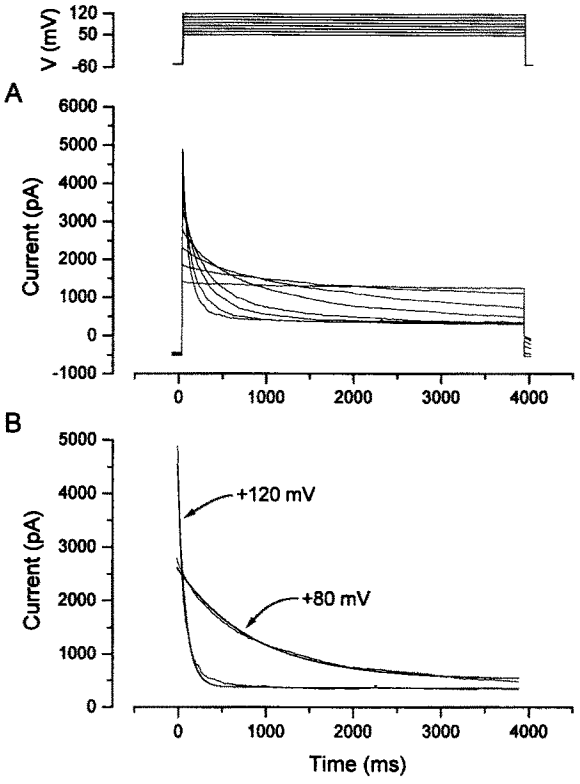

FIGURE 1. Kinetics of depolarization-induced inactivation of whole-cell current. Current inactivation was measured by voltage pulses to depolarizing membrane potentials. (*A*) Inactivation records from a single cell. Membrane potential was held at −50 mV and stepped to +50 to +120 mV for 4 s in 10-mV increments. The cell was allowed to recover at −50 mV for 10 s between voltage steps. Records were filtered at 0.5 kHz and digitized at 1 kHz. (*B*) Examples of single exponential fit to +80 and +120 mV current records obtained from cell shown in *A*. At +80 and +120 mV the parameters of the fit were τ = 862 ms and 92 ms, steady state inactivation = 80.5 and 92.4%, respectively.

1992) can be measured by fitting the data describing the voltage dependence of inactivation with the Boltzmann equation. A Boltzmann fit of the inactivation data is shown by the dashed line in Fig. 2 *B*. The parameters derived from the Boltzmann fit are inactivation midpoint = 68.6 mV; maximal inactivation = 87%; and effective gating charge = 3.42. Thus, the effective gating charge during an inactivation event is equivalent to 3–4 charges moving completely through the membrane potential field.

Voltage-dependent Reactivation

Reactivation of the channel after depolarization-induced inactivation was also voltage dependent. We characterized this reactivation behavior by stepping the membrane potential from a holding potential of −80 to +120 mV for 800 ms to induce channel inactivation. The membrane potential was then stepped to test potentials of −20 to −90 mV for 3 s. As shown in Figs. 3, *A* and *B*, membrane potential steps to hyperpolarizing voltages resulted in reactivation of the channel with a time course dependent on the membrane potential.

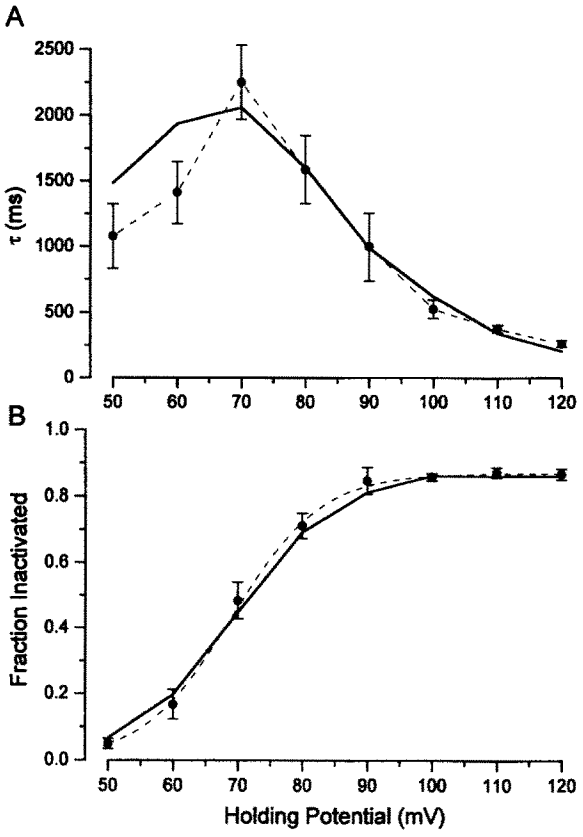

FIGURE 2. Parameters of depolarization-induced whole-cell current inactivation. Data from voltage step experiments (e.g., Fig. 1) were fit with single exponential decays. (*A*) Mean ± SE (n = 6) time constants at voltages from +50 to +120 mV (*Solid line*) The predicted time constants derived from the kinetic model. (*B*) Mean ± SE (n = 6) fractional inactivation level. The dashed line represents a fit to the data using the Boltzmann equation. The parameters derived from this fit were maximum inactivation level = 86%, inactivation midpoint = 69 mV and effective gating charge = 3.5. (*Solid line*) The predicted inactivation levels derived from the kinetic model.

The time course of reactivation could not be fit by a single exponential (Fig. 3 *B*, *dashed lines*). The data were fit adequately, however, by the sum of two exponentials (Fig. 3 *B* and Fig. 4). At all voltages tested, recovery was complete. The time constants for both the fast (τ_f) and slow (τ_s) components were voltage dependent and decreased as the potential became more hyperpolarized (Fig. 4, *A* and *B*). The fractional contribution (α) of the slow component to reactivation decreased slightly at more hyperpolarized potentials (Fig. 4 *C*).

pH Sensitivity of Voltage-dependent Inactivation

Fig. 5 shows the effect of extracellular pH on the τ and steady state inactivation induced by membrane depolarization. Reduction of bath pH to 5 greatly accelerated the time course of the inactivation process (Fig. 5 *A*) and shifted the midpoint of inactivation from 68.6 to 57.2 mV (Fig. 5 *B*). Elevation of external pH had the opposite effect, slowing inactivation and increasing the midpoint of inactivation to more depolarized voltages (Fig. 5 *B*). The midpoints of inactivation at pH 8 and 9 were 73.8 and 78.5 mV, respectively. Changing extracellular pH from 5–9 had no

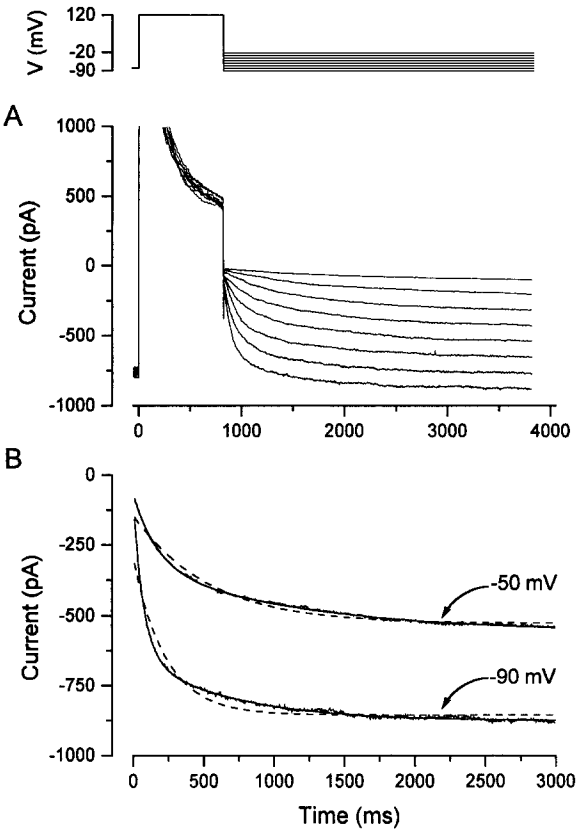

FIGURE 3. Voltage-dependent reactivation of whole-cell current. After depolarization-induced inactivation, whole cell current was reactivated in a voltage-dependent manner. (*A*) Reactivation record from a single cell. Cell was held at −80 mV, stepped to +120 mV for 800 ms to induce inactivation and then stepped to hyperpolarizing potentials from −20 to −90 mV for 3 s in 10-mV increments. Cell was allowed to recover for 7 s at −80 mV before subsequent depolarizing voltage steps. Records were filtered at 0.5 kHz and digitized at 1 kHz. (*B*) Reactivation records from A at −50 and −90 mV. (*Dotted and solid lines*) Single and double exponential fits to the data, respectively. The fast (τ_f) and slow time constants (τ_s) of reactivation were τ_f = 150 ms, τ_s = 1,062 ms at −50 mV and τ_f = 73 ms, τ_s = 662 ms at −90 mV.

inhibitory effect on the instantaneous whole-cell current measured at +60 mV (data not shown).

Boltzmann fits to the data shown in Fig. 5 *B* demonstrated that the rising part of the inactivation versus voltage curves became less steep as external pH increased. This indicates that the effective gating charge decreased with increasing pH. Fig. 5 *B* (*inset*) shows that the effective gating charge decreased from 4.2 at pH 5 to 2.4 at pH 8.

External ATP Block

Extracellular ATP inhibited the swelling-activated whole-cell anion conductance (Fig. 6). The ATP block was voltage dependent. No inhibition was observed at negative membrane potentials and the degree of blockage increased above the reversal potential of 0 mV (Fig. 6*A*). At +80 mV, 10 mM ATP inhibited the current 59.8 ± 5.6% (n = 3).

The block by external ATP dramatically altered depolarization-induced inactivation. The τ for inactivation at +120 mV in the presence of 10 mM ATP was >3 s (Fig. 7). At potentials < +100 mV, inactivation was not seen in the presence of ATP during 4-s depolarization steps (Fig. 7).

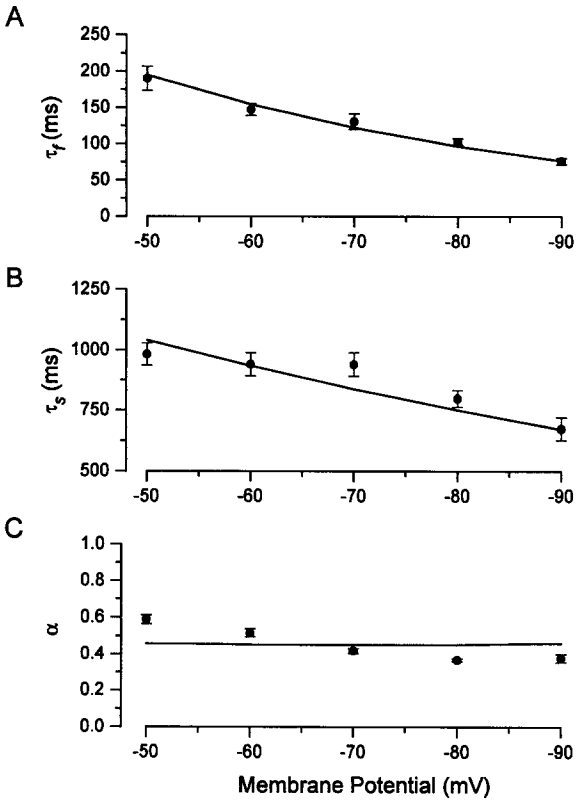

FIGURE 4. Parameters of voltage-dependent whole-cell current reactivation. Data from reactivation voltage steps (e.g., Fig. 3) were fit with double exponential decays. Three parameters were derived from this fit: fast (τ_f; *A*) and slow (τ_s; *B*) time constants and the fractional contribution of the slow component (α) to reactivation (*C*). Values shown are means ± SE (n = 9). The solid line in each panel shows the predicted values derived from the kinetic model.

The observed ATP block could be due to interaction of ATP with a binding site that alters channel structure or by a direct interaction of the nucleotide with the channel pore. To test whether ATP was interacting with the channel pore, we performed single-channel measurements. Fig. 8 illustrates the effect of 10 mM ATP on VSOAC current and single-channel events in an outside-out membrane patch. Three changes in the patch current are evident. First, the absolute magnitude of the current flow is substantially reduced by ATP similar to that seen in the whole cell. The estimated

unitary currents for the channels in this patch were 5.3 and 3.2 pA before and after exposure to 10 mM ATP, respectively. Second, ATP dramatically slowed the rate of channel inactivation. Third, the open-channel noise is greatly increased over that observed in the absence of ATP. The increase in open-channel noise is consistent with direct blockage of the channel pore by ATP.

If ATP is interacting directly with the channel pore, then the ATP block should be sensitive to the direction of Cl^- movement. We tested this idea by lowering intracellular Cl^- concentration from 140 to 40 mM. The mean Cl^- reversal potential

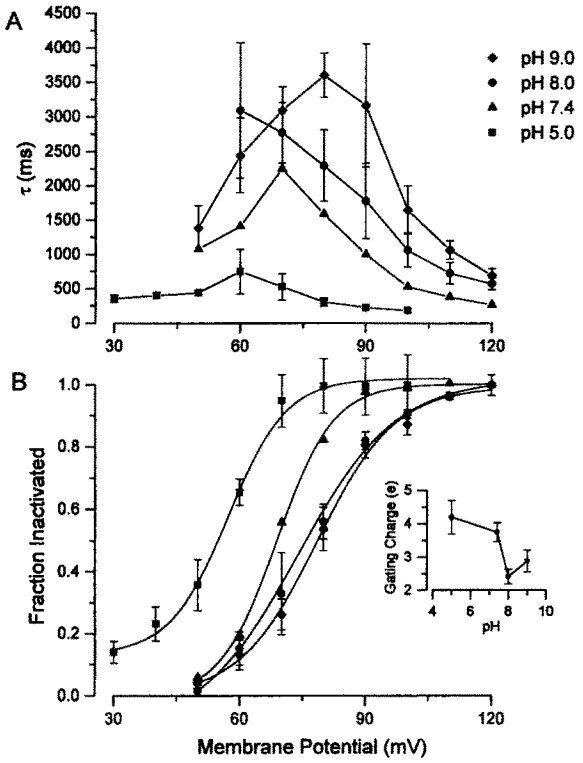

FIGURE 5. Effect of extracellular pH on depolarization-induced inactivation. (*A*) Decreases in external pH reduce the τ for inactivation. Time constants were determined by single exponential fits to depolarization-induced current inactivation records obtained at various pH values. Voltage pulse protocol was the same as in Fig. 1. (*B*) The midpoint of inactivation is shifted to less depolarized voltages by reductions in extracellular pH. Steady state inactivation data from experiments illustrated in *A* were normalized to the maximum fractional inactivation observed. Solid lines are Boltzmann fits to the data. (*Inset*) Effective gating charge, derived from the Boltzmann fits in *B*, decreases with increases in extracellular pH. Gating charge decreased from 4.2 at pH 5 to 2.4 at pH 8. Error bars are the standard errors of the gating charge parameter derived from the fitting routine. For all panels, the data obtained at pH 5, 8 and 9 are means ± SE (n = 4). Inactivation data at pH 7.4 are replotted from Fig. 2 without error bars for clarity.

was shifted from 0 mV to −25.8 ± 3 mV (±SE, n = 5) by this experimental maneuver. As shown in Fig. 6 *B*, inhibition was observed at all membrane potentials more positive than the reversal potential of −31 mV in this cell. Identical results were obtained in measurements made on four separate cells (data not shown). At +80 mV, ATP inhibited the current by 43.7 ± 2% (mean ± SE, n = 5). These results demonstrate that ATP blocks by interacting with the channel pore rather than an external

binding site. Presumably, net Cl^- movement out of the cell has a sweeping away effect that prevents ATP from entering and blocking the channel pore (e.g., Armstrong, 1971).

Modeling and Simulation of Voltage Sensitivity

Insights into the molecular events that underlie the voltage-dependent behavior of VSOAC can be obtained by developing kinetic models. While many different models that fit the data adequately could probably be developed, the simplest and most

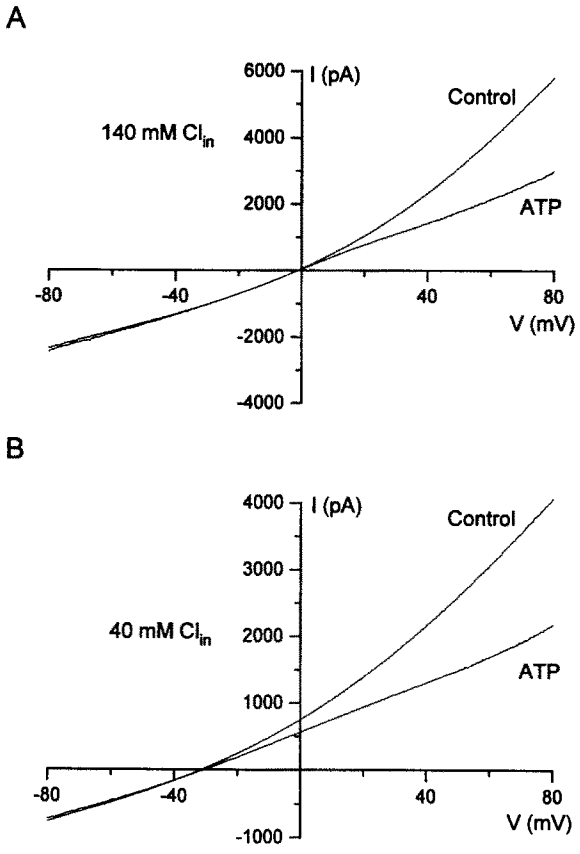

FIGURE 6. Extracellular ATP blocks VSOAC in a voltage-dependent manner. Current-to-voltage relationships were measured by subjecting cells to voltage ramps from −60 to +60 mV (60 mV/s). Each panel shows current-to-voltage relationships before and after application of 10 mM Na_2ATP to the external bath. (*A*) Current-to-voltage relationship with 140 mM CsCl in the bath and patch pipette solution. (*B*) Current-to-voltage relationship with 140 mM CsCl in the bath and 40 mM CsCl in the patch pipette solution. CsCl in the patch pipette was replaced isosmotically with raffinose.

useful starting point is to consider a linear scheme where the channel exists in one open and one or more inactivated states. We assume that the rate constants governing the transition between states are exponentially dependent on membrane voltage and are described by

$$k(V) = k_0 e^{AV} \tag{1}$$

where $k(V)$ is the rate constant, V is the voltage in mV, A is a constant that determines voltage sensitivity and k_0 is the rate constant at 0 mV (Stevens, 1978). Assuming that

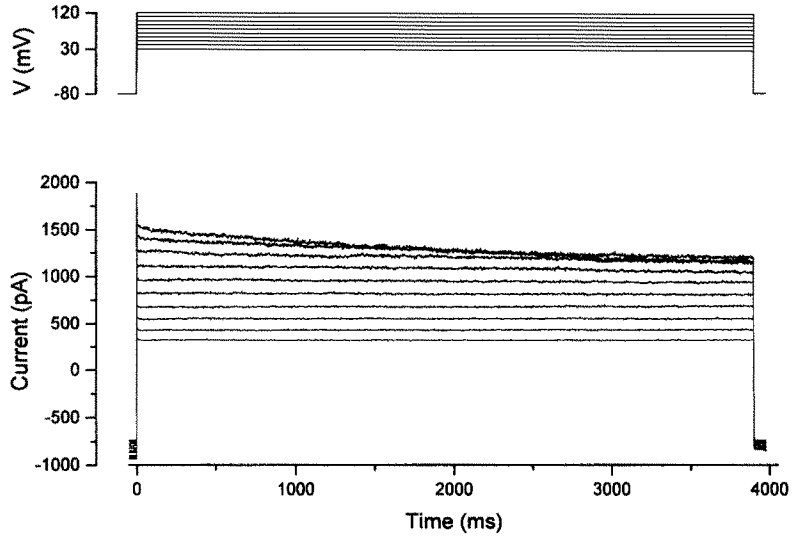

FIGURE 7. Extracellular ATP slows depolarization-inactivation. Cells were held at −80 mV and stepped to depolarizing potentials between +30 and +120 mV for 4 s in 10-mV increments. Cells were allowed to recover for 10 s between voltage steps. Records were filtered at 0.5 kHz and digitized at 1 kHz. Cells were exposed to 10 mM Na_2ATP in the external bath solution. Inactivation was not seen at voltages < +100 mV. At +120 mV the τ for inactivation was > 3 s.

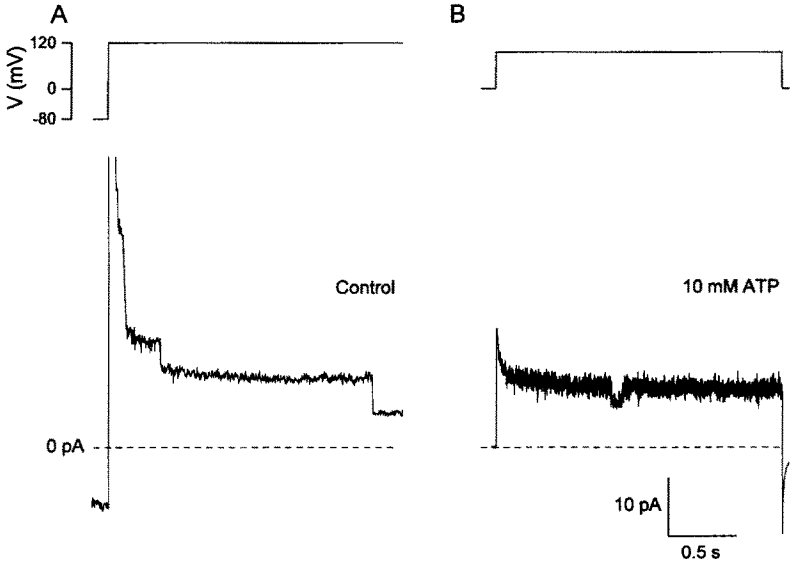

FIGURE 8. Extracellular ATP reduces single-channel current and slows channel inactivation in outside-out membrane patches. Outside-out patches were pulled from swollen cells, held at −80 mV and pulsed to +120 mV for 2 s. Exposure to 10 mM Na_2ATP reduces patch and single-channel current, increases open-channel noise and dramatically slows inactivation. Records were filtered at 0.5 kHz and digitized at 1 kHz. The estimated unitary currents for the channels in this patch were 5.3 and 3.2 pA before and after exposure to ATP, respectively. Single-channel currents were estimated from depolarization-induced channel closures (*control*) and the single transient closures observed in the presence of extracellular ATP.

TABLE I

Parameters of the Kinetic Model

Rate constant	k_0	A	q
	s^{-1}	mV^{-1}	
k_1	0.0231	0.045	1.129
k_{-1}	40.76	−0.04	−1.004
k_2	0.194	0.0285	0.715
k_{-2}	1.58	−0.235	−0.590
k_3	0.0176	0.035	0.878
k_{-3}	0.553	−0.011	−0.276

these transitions between the various states obey absolute rate theory, the effective gating charge q is related to the voltage sensitivity A according to

$$q = AkT/e \tag{2}$$

where k is the Boltzmann constant, T is the absolute temperature, and kT/e = 25.3 mV at 20°C.

Kinetic models were developed by manually adjusting the parameters defined in Eq. 1 to best fit the observed data. A linear model with one inactivated state did not

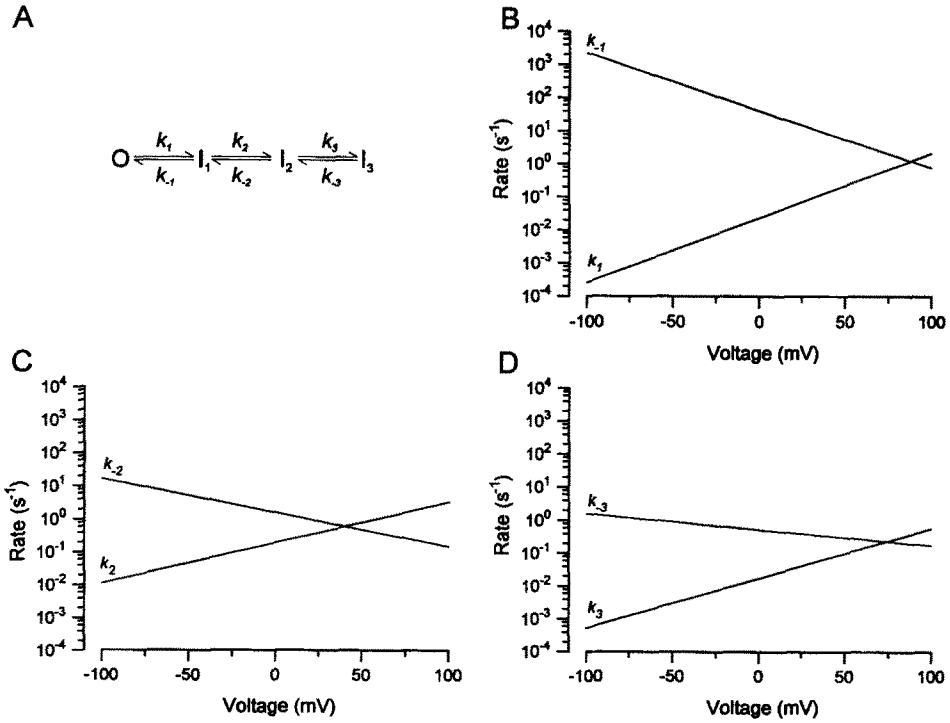

FIGURE 9. Effect of voltage on rate constants derived for the kinetic model. The model is shown in *A*. Rates are shown for transition 1 in *B*, 2 in *C*, and 3 in *D*. Values for k_0, A and q are listed in Table I.

reproduce the double exponential nature of voltage-dependent channel reactivation. A linear model with two inactivated states produced double exponential reactivation kinetics. This model, however, could not simultaneously account for the voltage sensitivity of both inactivation and reactivation. The kinetic scheme shown below with one open (O) and three inactivated (I) states accounted for all of our whole-cell data.

$$O \underset{k_{-1}}{\overset{k_1}{\rightleftharpoons}} I_1 \underset{k_{-2}}{\overset{k_2}{\rightleftharpoons}} I_2 \underset{k_{-3}}{\overset{k_3}{\rightleftharpoons}} I_3$$

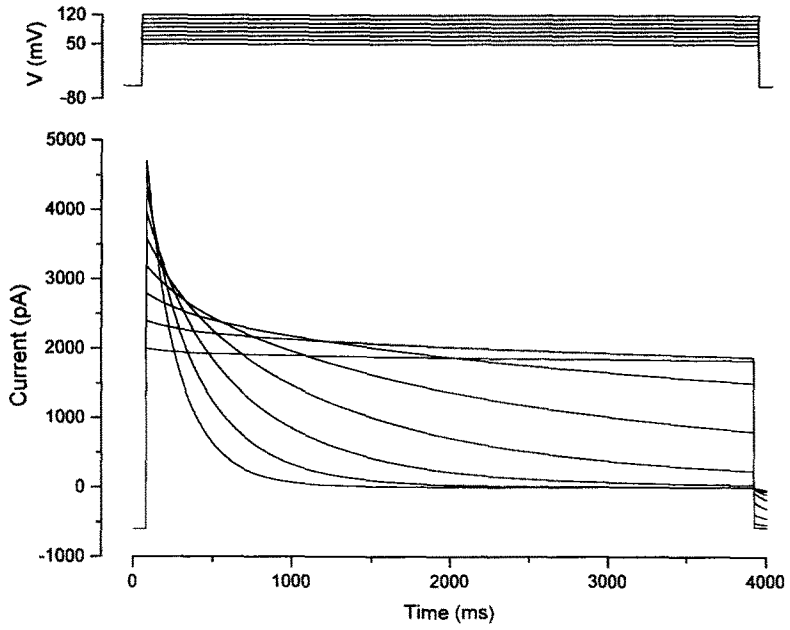

FIGURE 10. Simulation of depolarization-induced inactivation. Whole-cell currents were simulated using the four state linear model described in the text and voltage-dependent rate constants from Table I. The number of channels was assumed to be 10,000 and the single-channel conductance 40 pS at positive voltages and 10 pS at negative voltages (see Jackson and Strange, 1995).

The parameters that best fit the observed data are shown in Table I and Fig. 9 for each of the six voltage-dependent rate constants. A simulation of voltage-dependent inactivation is shown in Fig. 10. These model traces were fit well with single exponential decays and yielded time constants and fractional inactivations that were in excellent agreement with the observed data (Fig. 2, *solid lines*).

Simulation of voltage-dependent reactivation is shown in Fig. 11. These model traces were well fit by double exponentials. The fits yielded time constants that were in excellent agreement with the whole cell data. The fit to the fractional contribution of the slow component to reactivation (α) was also in good agreement with the whole cell data. However, the slight decline in α was not predicted by the model (Fig. 4, *solid lines*).

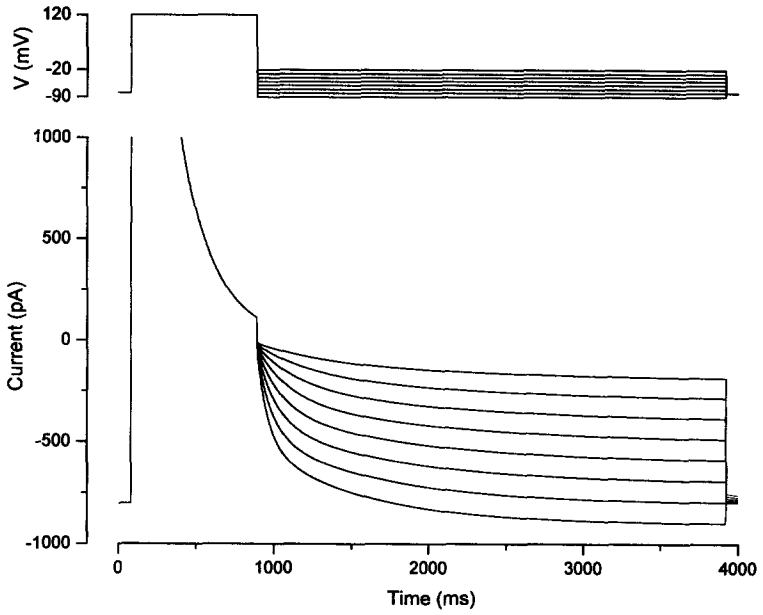

FIGURE 11. Simulation of voltage-dependent reactivation. Whole-cell currents were simulated using the four-state linear model described in the text and voltage-dependent rate constants from Table I. The number of channels was assumed to be 10,000 and the single-channel conductance 40 pS at positive voltages and 10 pS at negative voltages (see Jackson and Strange, 1995).

DISCUSSION

Kinetic Model of the Voltage-dependent Properties of VSOAC

A simple linear kinetic model of the voltage-dependent properties of VSOAC was developed by characterizing depolarization-induced inactivation of whole-cell currents. Linear kinetic schemes with one open state and either one or two inactivated states did not adequately simulate the voltage-dependent behavior of VSOAC. A kinetic scheme where the channel shifts between one open and three inactivated states, however, provided excellent fits to all of the whole-cell data. As stated previously, there are probably several models which could explain the voltage sensitivity of VSOAC. Our analysis, however, serves to set a limit on the minimum number of inactivated states required to account for channel gating kinetics.

The time course of depolarization-induced inactivation of VSOAC in C6 cells is well fit by a single exponential (Fig. 1). Our model predicts that with one open and three inactivated states deviation from single-exponential behavior will be small (Figs. 2 and 10). In other words, the kinetics of inactivation are dominated by transitions of the channel from a single open state into the first inactivated state.

Similarly, our model predicts the observed double exponential reactivation kinetics (Figs. 3 and 11). These kinetics largely represent reactivation of channels in the second and third inactivated states. Transition of the channel from the first

inactivated state to the open state is more rapid and thus not rate limiting for reactivation.

The range of effective gating charges (Table I) predicted by the model are comparable to those observed for other channels such as the squid axon Na^+ channel (Vandenberg and Bezanilla, 1991) and the fast Cl^- channel in rat skeletal muscle (Weiss and Magleby, 1992). In contrast, the rate constants at 0 mV (k_o) for VSOAC (Table I) are generally much smaller than those for either of these channel types. This is consistent with the fact that the gating kinetics of the axon Na^+ channel and skeletal muscle Cl^- channel are much faster than those of VSOAC.

pH Sensitivity of Depolarization-induced Inactivation

Extracellular acidification decreases the time constant for depolarization-induced inactivation of the endogenous swelling-activated anion current in *Xenopus* oocytes (Ackerman et al., 1994). A similar effect of pH is observed in C6 glioma cells (Fig. 5). Acidification increases the rate of inactivation and shifts the midpoint of inactivation to less positive voltages (Fig. 5 *B*). As shown in Fig. 5 *B* (*inset*), acidification also increases the effective gating charge. Titration of negative surface charge with protons should shift the voltage dependence of inactivation to more depolarized voltages without altering effective gating charge (e.g., Woodhull, 1973; Krafte and Krass, 1988; Zhang and Seigelbaum, 1991). Thus, the effects of pH on VSOAC inactivation kinetics indicates that amino acid residues on the channel protein are being titrated.

Decreases in gating charge with alkalinization indicates that basic amino acid residues on the voltage sensor are being titrated. The pH range over which the titration occurs (pH 5–8; Fig. 5 *B* [*inset*]) implies that protons are titrating histidine residues (pK_a 6.0) rather than more basic arginine (pK_a 12.5) or lysine (pK_a 10.5) residues. The shape of the titration curve in Fig. 5 *B*, however, is complex and suggests that more than a single, titratable amino acid residue participates in voltage-dependent gating of VSOAC. Additional studies are needed to fully understand the effects of protons on channel voltage sensitivity.

Voltage-dependent ATP Block

Exposure to extracellular nucleotides such as ATP inhibits the endogenous swelling-activated anion current in *Xenopus* oocytes (Ackerman et al., 1994) and the anion current induced by overexpression of I_{Cln} (Paulmichl, Li, Wickman, Ackerman, Peralta, and Clapham, 1992). Similarly, we found that whole cell VSOAC current (Fig. 6), as well as single channel currents (Fig. 8; see also Jackson and Strange, 1995), were blocked by extracellular ATP in C6 glioma cells.

The inhibition of VSOAC by extracellular ATP is voltage-dependent and sensitive to the direction of net Cl^- movement (Fig. 6). Exposure to extracellular ATP also dramatically increases open-channel noise (Fig. 8). Taken together, these results indicate that ATP inhibits VSOAC by interacting directly with the channel pore.

The electrophysiological characteristics of VSOAC are identical to those of the putative I_{Cln} channel (Paulmichl et al., 1992). We have suggested previously that VSOAC is a porin-like channel that may be coded for by the I_{Cln} gene (Jackson and Strange, 1995; Strange and Jackson, 1995). Interestingly, the I_{Cln} channel is blocked

by extracellular application of ATP and other nucleotides. Paulmichl et al. (1992) identified a putative nucleotide binding site that lies within the predicted pore region near the extracellular mouth of the I_{Cln} channel. These results are consistent with our conclusion that ATP functions as an open channel blocker.

Blockage of VSOAC by ATP dramatically slows depolarization-induced inactivation (Fig. 7). Inhibition of voltage-dependent channel closure by permeant ions has been referred to previously as the foot-in-the-door effect (Swenson and Armstrong, 1981). If inactivation of VSOAC is due to the movement of a gate or flap into the pore (Hille, 1992), ATP may bind near this structure and hinder its movement. Alternatively, channel closure might occur by large scale macromolecular changes with resultant pore constriction (e.g., Unwin and Ennis, 1984; Zimmerberg and Parsegian, 1990). Pore constriction could be blocked by the presence of a large ATP molecule in the pore lumen.

We thank Dr. Kari Nadeau for critical reading of the manuscript, Dr. Bruce Bean for helpful and stimulating discussions, and Cambridge Neuroscience for technical assistance.

This work was supported by NIH grants NS30591 and DK45628. K. Strange is an Established Investigator of the American Heart Association. P. Jackson was supported by the Boston Neurosurgical Foundation and by NIH training grant T32EY07110.

Original version received 11 October 1994 and accepted version received 5 January 1995.

REFERENCES

Ackerman, M. J., K. D. Wickman, and D. E. Clapham. 1994. Hypotonicity activates a native chloride current in *Xenopus* oocytes. *Journal of General Physiology.* 103:153–179.

Armstrong, C. M. 1971. Interaction of tetraethylammonium ion derivatives with the potassium channels of giant axons. *Journal of General Physiology.* 58:413–437.

Chan, H.-C., J. Goldstein, and D. J. Nelson. 1992. Alternate pathways for chloride conductance activation in normal and cystic fibrosis airway epithelial cells. *American Journal of Physiology.* 262:C1273–C1283.

Garcia-Perez, A., and M. B. Burg. 1991. Renal medullary organic osmolytes. *Physiological Reviews.* 71:1081–1115.

Hallows, K. R., and P. A. Knauf. 1994. Principles of cell volume regulation. *In* Cellular and Molecular Physiology of Cell Volume Regulation. K. Strange, editor. CRC Press, Boca Raton, FL. 3–29.

Hille, B. 1992. Ionic Channels of Excitable Membranes. Second edition. Sunderland Associates, Inc., Sunderland, MA. 312 pp.

Jackson, P. S., and K. Strange. 1993. Volume-sensitive anion channels mediate swelling-activated inositol and taurine efflux. *American Journal of Physiology.* 265:C1489–C1500.

Jackson, P. S., and K. Strange. 1995. Single channel properties of a volume-sensitive anion conductance. Current activation occurs by abrupt switching of closed channels to an open state. *Journal of General Physiology.* 105:643–660.

Jackson, P., R. Morrison, and K. Strange. 1994. The volume-sensitive organic osmolyte-anion channel VSOAC is regulated by non-hydrolytic ATP binding. *American Journal of Physiology.* 267:C1203–C1209.

Krafte, D. S., and R. S. Kass. 1988. Hydrogen ion modulation of a Ca channel current in cardiac ventricular cells. Evidence for multiple mechanisms. *Journal of General Physiology.* 91:641–657.

Kubo, M., and Y. Okada. 1992. Volume-regulatory Cl^- channel currents in cultured human epithelial cells. *Journal of Physiology.* 456:351–371.

Lewis, R. S., P. E. Ross, and M. D. Cahalan. 1993. Chloride channels activated by osmotic stress in T lymphocytes. *Journal of General Physiology.* 101:801–826.

McCann, J. D., M. Li, and M. J. Welsh. 1989. Identification and regulation of whole-cell chloride currents in airway epithelium. *Journal of General Physiology.* 94:1015–1036.

Okada, Y., C. C. H. Petersen, M. Kubo, S. Morishima, and M. Tominaga. 1994. Osmotic swelling activates intermediate-conductance Cl^- channels in human intestinal epithelial cells. *Japanese Journal of Physiology.* 44:403–409.

Paulmichl, M., Y, Li, K. Wickman, M. Ackerman, E. Peralta, and D. Clapham. 1992. New mammalian chloride channel identified by expression cloning. *Nature.* 356:238–241.

Pollard, C. E. 1993. A volume-sensitive Cl^- conductance in a mouse neuroblastoma X rat dorsal root ganglion cell line (F11). *Brain Research.* 614:178–184.

Rugolo, M., T. Mastrocola, M. De Luca, G. Romeo, and L. J. V. Galietta. 1992. A volume-sensitive chloride conductance revealed in cultured human keratinocytes by $^{36}Cl^-$ efflux and whole-cell patch clamp recording. *Biochimica et Biophysica Acta.* 1112:39–44.

Solc, C. K., and J. J. Wine. 1991. Swelling-induced and depolarization-induced Cl^- channels in normal and cystic fibrosis epithelial cells. *American Journal of Physiology.* 261:C658–C674.

Stevens, C. F. 1978. Interactions between intrinsic membrane protein and electric field. An approach to studying nerve excitability. *Biophysical Journal.* 22:295–306.

Stoddard, J. S., J. H. Steinbach, and L. Simchowitz. 1993. Whole cell Cl^- currents in human neutrophils induced by cell swelling. *American Journal of Physiology.* 265:C156–C165.

Strange, K. 1994. Are all cell volume changes the same? *News in Physiological Sciences.* 9:223–228.

Strange, K., and P. S. Jackson. 1995. Swelling-activated organic osmolyte efflux: a new role for anion channels. *Kidney International.* In press.

Strange, K., K. Churchwell, N. Ballatori, J. L. Boyer, and P. S. Jackson. 1995. Properties of volume-sensitive organic osmolyte/anion channels (VSOAC) in hepatocytes of the marine skate *Raja erinacea. Federation of American Societies of Experimental Biology Journal.* 9:A636. (Abstr.)

Swenson, R. P., and C. M. Armstrong. 1981. K^+ channels close more slowly in the presence of external K^+ and Rb^+. *Nature.* 291:427–429.

Tseng, G.-N. 1992. Cell swelling increases membrane conductance of canine cardiac cells: evidence for a volume-sensitive Cl channel. *American Journal of Physiology.* 262:C1056–C1068.

Unwin, P. N. T., and P. D. Ennis. 1984. Two configurations of a channel-forming membrane protein. *Nature.* 307:609–613.

Vandenberg, C. A., and F. Bezanilla. 1991. A sodium channel gating model based on single channel macroscopic ionic, and gating currents in the squid giant axon. *Biophysical Journal.* 60:1511–1533.

Weiss, D. S., and K. L. Magelby. 1992. Voltage-dependent gating mechanism for single fast chloride channels from rat skeletal muscle. *Journal of Physiology.* 453:279–306.

Woodhull, A. M. 1973. Ionic blockage of sodium channels in nerves. *Journal of General Physiology.* 61:687–708.

Worrell, R. T., A. G. Butt, W. H. Cliff, and R. A. Frizzell. 1989. A volume-sensitive chloride conductance in human colonic cell line T84. *American Journal of Physiology.* 256:C1111–C1119.

Yancey, P. H. 1994. Compatible and counteracting solutes. *In* Cellular and Molecular Physiology of Cell Volume Regulation. K. Strange, editor. CRC Press, Boca Raton, FL. 81–109.

Zhang, J.-F., and S. A. Siegelbaum. 1991. Effects of external protons on single cardiac sodium channels from guinea pig ventricular myocytes. *Journal of General Physiology.* 98:1065–1083.

Zimmerberg, J., and V. A. Parsegian. 1986. Polymer inaccessible volume changes during opening and closing of a voltage-dependent ionic channel. *Nature.* 323:36–39.